

# Calibrating a long-term meteoric $^{10}\text{Be}$ delivery rate into eroding Western US glacial deposits by comparing meteoric and in situ-produced $^{10}\text{Be}$ depth profiles

5 Travis Clow<sup>1</sup>, Jane K. Willenbring<sup>1,2</sup>, Mirjam Schaller<sup>3</sup>, Joel D. Blum<sup>4</sup>, Marcus Christl<sup>5</sup>, Peter W. Kubik<sup>5</sup>, Friedhelm von Blanckenburg<sup>2</sup>

<sup>1</sup>Department of Geological Sciences, Stanford University, Stanford, CA, USA

<sup>2</sup>GFZ German Research Centre for Geosciences, Earth Surface Geochemistry, Telegrafenberg, 14473 Potsdam, Germany

10 <sup>3</sup>Geodynamics, University of Tübingen, Wilhelmstraße 56, 72076 Tübingen, Germany

<sup>4</sup>Department of Earth and Environmental Sciences, University of Michigan, Ann Arbor, MI, USA

<sup>5</sup>ETH Zurich, Laboratory of Ion Beam Physics, HPK G23, Schafmattstrasse 20, ETH-Zurich, CH-8093 Zurich, Switzerland

Correspondence to: Travis Clow (tclow@stanford.edu)

**Abstract.** Meteoric  $^{10}\text{Be}$  ( $^{10}\text{Be}_{\text{met}}$ ) concentrations in soil profiles have great potential as a geochronometer and a tracer of  
15 Earth surface processes, particularly in fine-grained soils lacking quartz that would preclude the use of *in situ*-produced  $^{10}\text{Be}$  ( $^{10}\text{Be}_{\text{in situ}}$ ). One prerequisite for using this technique for accurately calculating rates and dates is constraining the delivery, or flux, of  $^{10}\text{Be}_{\text{met}}$  to a site. However, few studies to date have quantified long-term (i.e. millennial) delivery rates, and none have determined a delivery rate for an eroding soil. In this study, we compared existing concentrations of  $^{10}\text{Be}_{\text{in situ}}$  with new measurements of  $^{10}\text{Be}_{\text{met}}$  in eroding soils sampled from the same depth profiles to calibrate a long-term  $^{10}\text{Be}_{\text{met}}$  delivery rate.  
20 We did so on the Pinedale (~21-25 ky) and Bull Lake (~140 ky) glacial moraines at Fremont Lake, Wyoming (USA) where age, grain sizes, weathering indices, and soil properties are known, as are erosion/denudation rates calculated from  $^{10}\text{Be}_{\text{in situ}}$ . After ensuring sufficient beryllium retention in each profile, solving for the delivery rate of  $^{10}\text{Be}_{\text{met}}$ , and normalizing for paleomagnetic and solar intensity variations over the Holocene, we calculate  $^{10}\text{Be}_{\text{met}}$  fluxes of  $1.46 (\pm 0.20) \times 10^6$  atoms  $\text{cm}^{-2} \text{y}^{-1}$  and  $1.30 (\pm 0.48) \times 10^6$  atoms  $\text{cm}^{-2} \text{y}^{-1}$  to the Pinedale and Bull Lake moraines, respectively, and compare these values to  
25 two widely-used  $^{10}\text{Be}_{\text{met}}$  delivery rate estimation methods that substantially differ for this site. Accurately estimating  $^{10}\text{Be}_{\text{met}}$  flux using these methods requires consideration of spatial scale as well as temporally varying parameters (i.e. paleomagnetic field intensity, solar modulation) to ensure the most realistic estimates of  $^{10}\text{Be}_{\text{met}}$ -derived erosion rates in future studies.

## 1 Introduction

<sup>10</sup>Be is a cosmogenic isotope with a half-life of 1.39 +/- 0.01 My (Chmeleff et al., 2010) and its meteoric form (<sup>10</sup>Be<sub>met</sub>) is produced in the atmosphere through spallation reactions as high-energy cosmic rays collide with target nuclei (i.e. <sup>14</sup>N and <sup>16</sup>O) in the atmosphere (Lal and Peters, 1967). <sup>10</sup>Be<sub>met</sub> is then delivered to Earth's surface via precipitation or as dry deposition at a flux of 0.1 – 2 x 10<sup>6</sup> atoms cm<sup>-2</sup> y<sup>-1</sup> followed by dissolved export in runoff, or depending on retentivity, adsorption onto fine-grained, reactive surfaces, typically clays and Fe- and Al-oxyhydroxides in soil horizons at the Earth's surface (Graly et al., 2010; Willenbring and von Blanckenburg, 2010). <sup>10</sup>Be<sub>met</sub> has been used as a tracer of Earth surface processes, including estimating erosion rates at the soil-profile and river-catchment scales, soil residence times, ages of landforms over millennial to million-year timescales, and paleo-denudation rates from marine sedimentary records (Pavich et al., 1986; McKean et al., 1993; Jungers et al., 2009; Willenbring and von Blanckenburg, 2010; von Blanckenburg et al., 2012; von Blanckenburg and Bouchez, 2014; Wittman et al., 2015; von Blanckenburg et al., 2015; Portenga et al., 2019; Jelinski et al., 2019). Prerequisites for interpreting the concentrations and isotope ratios (i.e. <sup>10</sup>Be<sub>met</sub>/<sup>9</sup>Be) as erosion or denudation (the sum of erosion and weathering) rates, respectively, include knowing the delivery rate of <sup>10</sup>Be<sub>met</sub> (Pavich et al., 1986; Reusser et al., 2010; Graly et al., 2011; Heikkilä and von Blanckenburg, 2015; Dixon et al., 2018, Deng et al., 2020) and quantifying the mobility or retention of beryllium in soils (e.g. Bacon et al., 2012; Boschi and Willenbring, 2016a,b; Maher and von Blanckenburg, 2016; Dixon et al., 2018), not all of which was possible in many previous studies. The potential ability of using <sup>10</sup>Be<sub>met</sub> depth profiles to obtain quantitative data on soil ages, residence times, production- and denudation rates in a similar manner as *in situ*-produced <sup>10</sup>Be (<sup>10</sup>Be<sub>in situ</sub>) depth profiles could prove to be highly advantageous, as it is easier to measure (due to much higher concentrations than <sup>10</sup>Be<sub>in situ</sub>) and can be employed in a much wider range of environments, as there is no dependence on the existence of coarse-grained quartz as is required for the analysis of <sup>10</sup>Be<sub>in situ</sub>. <sup>10</sup>Be<sub>in situ</sub> shares a cosmic ray origin with <sup>10</sup>Be<sub>met</sub> but differs in production method; <sup>10</sup>Be<sub>in situ</sub> is produced within crystal lattices in surface rocks and soil, rather than in the atmosphere, with a well constrained total production rate of 4.01 atoms g<sup>-1</sup>y<sup>-1</sup> at sea level, high latitude (Borchers et al., 2016), and is characterized by full retentivity and known production pathways with depth. <sup>10</sup>Be<sub>met</sub>, in stark contrast, is potentially subjected to variable adsorption depths, incomplete retentivity, and heterogeneous internal redistribution.

In this study, we compare the previously published  $^{10}\text{Be}_{\text{in situ}}$  depth profiles of the Pinedale and Bull Lake terminal glacial moraines in Wind River, Wyoming (Schaller et al., 2009a,b) with new  $^{10}\text{Be}_{\text{met}}$  concentrations from depth profiles from the same sample material to evaluate the long-term (i.e. millennial) delivery rate of  $^{10}\text{Be}_{\text{met}}$  ( $F(^{10}\text{Be}_{\text{met}})$ ) to this site. This is the first study that evaluates  $F(^{10}\text{Be}_{\text{met}})$  for eroding soils as derived from the comparison of  $^{10}\text{Be}_{\text{in situ}}$  and  $^{10}\text{Be}_{\text{met}}$  depth profiles and erosion rates. We utilize previous knowledge of effective transient erosion rates from Schaller et al. (2009a), recalculated with revised parameters for *in situ* production of  $^{10}\text{Be}$ , to constrain and locally calibrate  $F(^{10}\text{Be}_{\text{met}})$  to these moraines while considering the extent of  $^{10}\text{Be}_{\text{met}}$  retention post-delivery. We then compare the resulting calculated  $F(^{10}\text{Be}_{\text{met}})$ , with propagated uncertainties, with the predicted  $F(^{10}\text{Be}_{\text{met}})$  of Graly et al. (2011) and Heikkilä and von Blanckenburg (2015), normalizing each result for paleomagnetic field intensity variations over the Holocene. We also explore the practical differences between these flux estimates and advocate for each approach to be carried out when estimating  $F(^{10}\text{Be}_{\text{met}})$  for use in erosion rate calculations in future studies.

## 2 Background

### 2.1 Study Area

The Fremont Lake area of the Wind River Mountains (Wyoming, United States) experienced multiple glacial advances during the Pleistocene, evidenced by several moraines of Pinedale and Bull Lake age (Fig. 1; modified from original mapping and descriptions by Richmond, 1973). The climate is cold, semi-arid, and windy, with a 50-year precipitation rate and temperature of  $27.6 \text{ cm y}^{-1}$  and  $2.1^\circ \text{ C}$ , respectively (WRCC, 2005), in the nearby town of Pinedale, Wyoming (~3.5 km southwest of the field area).

The Pinedale and Bull Lake age terminal moraines (hereafter referred to as Pinedale and Bull Lake moraines) analyzed in this study (Fig. 1) were formed by highland-to-valley mountain glaciers draining an ice cap accumulation zone that covered the mountain range. The Pinedale moraine is more steep-sided and boulder-strewn than the gently sloping Bull Lake

moraine, each with a total height of ~30 m (see Figs. 1b, 1c of Schaller et al., 2009a for detailed moraine transects). The pH of the moraine soils is well characterized; both profiles have pedogenic carbonate below 1 m, fixing the pH at depth to ~ 8 (Chadwick and Chorover, 2001). Hall and Shroba (1995) report pH data on profiles adjacent to those analyzed in this study, with average pH ranging from ~5.5 on the surface to ~8 at depth.

80

The depth profile samples analyzed for  $^{10}\text{Be}_{\text{met}}$  reported here are the same sample material analyzed for  $^{10}\text{Be}_{\text{in situ}}$  by Schaller et al. (2009a). We utilize bulk samples sieved to <2 mm for our analysis, extracted from the lower mineral soil developed on each moraine, both mixtures of reworked glacial till (composed of Archean granite, granodiorite, and dioritic gneiss) that have a high likelihood for inheritance from cosmic ray exposure prior to burial. The same reported depths and grain size distributions apply for each sample at depth. The primary mineral content in the deepest (unweathered, >2 mm size fraction) sample is (in order of decreasing abundance): plagioclase, quartz, biotite, K-feldspar, hornblende, and magnetite (Taylor and Blum, 1995). Secondary clay minerals in the <2  $\mu\text{m}$  size fraction include kaolinite, vermiculite, illite, and smectite (Mahaney and Halvorson, 1986), with total clay content ranging from 3 to 10 wt% and 9 to 30 wt% for the Pinedale and Bull Lake profiles, respectively. Major element data is reported in Schaller et al. (2009b). Sr isotope measurements of the moraine soils and dust sources showed insignificant dust fluxes in the depth profiles of the Pinedale and Bull Lake moraines (Blum and Erel, 1997; Taylor and Blum, 1997).

90

## 2.2 Independent $^{10}\text{Be}_{\text{met}}$ Flux Estimation

Accurately estimating  $F(^{10}\text{Be}_{\text{met}})$  from field experiments is a topic of ongoing debate (e.g. Ouimet et al., 2015; Dixon et al., 2018), particularly in regard to the effect of precipitation rate on the flux (i.e. whether precipitation leads to additive or dilution effects on delivered  $^{10}\text{Be}_{\text{met}}$ , see *Willenbring and von Blanckenburg (2010)* and *Deng et al. (2020)* for extensive reviews).  $F(^{10}\text{Be}_{\text{met}})$  also varies through time, depending on solar modulation and paleomagnetic field intensity, and has a spatial distribution primarily resulting from atmospheric mixing and scavenging. One means to estimate  $^{10}\text{Be}_{\text{met}}$  production and delivery are  $F(^{10}\text{Be}_{\text{met}})$  estimates based on global atmospheric models (Field et al., 2006; Heikkilä and von Blanckenburg, 2015), which provide an estimate over large spatial scales. Another type of estimate is based on empirical, precipitation-

100 dependent field estimates of  $^{10}\text{Be}_{\text{met}}$  inventories in dated soils (Graly et al., 2011) measured over annual time scales. The work of Ouimet et al. (2015) highlighted the necessity for local  $F(^{10}\text{Be}_{\text{met}})$  estimates that also integrate over millennial time scales against models such as these, as their comparison of  $^{10}\text{Be}_{\text{met}}$  inventories and deposition rates from Pinedale- and Bull Lake-aged landforms in the Colorado Front Range showed that some were lower, and some exceeded, deposition rates from atmospheric models and precipitation collections.

105

The  $F(^{10}\text{Be}_{\text{met}})$  map of Heikkilä and von Blanckenburg (2015) utilizes the  $^{10}\text{Be}_{\text{met}}$  production functions of Masarik and Beer (1999) combined with the ECHAM5 general circulation model (GCM). Production rates were scaled to reflect the solar modulation and magnetic field strength for the entire Holocene (280.94 MV) using measured  $^{10}\text{Be}$  concentrations in ice cores. The authors ultimately present a global grid of predicted “pre-industrial” and “industrial” (referring to simulated aerosol and greenhouse gas concentrations) Holocene  $F(^{10}\text{Be}_{\text{met}})$  with an approximate cell size of 300 km x ~230 km. GCMs such as this are useful for modeling atmospheric mixing of  $^{10}\text{Be}_{\text{met}}$ , particularly in the stratosphere, as well as the regional effect of climate and its influence on  $F(^{10}\text{Be}_{\text{met}})$  via atmospheric circulation and precipitation (Heikkilä et al., 2012). At this latitude (~42.9° N), the pre-industrial predicted  $F(^{10}\text{Be}_{\text{met}})$  of  $1.38 \times 10^6$  atoms  $\text{cm}^{-2} \text{y}^{-1}$  is nearly identical to that derived from the flux map of Field et al. (2006), which utilizes the GISS (Goddard Institute for Space Studies Model E) GCM to model production. We use the pre-industrial modeled  $F(^{10}\text{Be}_{\text{met}})$  in our comparisons, as it is a more appropriate estimate for landforms of these ages. To place an upper bound uncertainty on this estimate, which is otherwise hard to quantify, we utilize the difference between the industrial and pre-industrial predicted  $F(^{10}\text{Be}_{\text{met}})$  ( $+0.99 \times 10^6$  atoms  $\text{cm}^{-2} \text{y}^{-1}$ ). This difference is solely a result of climate-dependent shifts in the delivery of  $^{10}\text{Be}_{\text{met}}$  and shifts resulting from large industrial aerosol loading in modern times and does not reflect changes in atmospheric production (Heikkilä and von Blanckenburg, 120 2015).

On the other hand, the empirical, present-day estimates of  $F(^{10}\text{Be}_{\text{met}})$  from Graly et al. (2011) are based on measurements of  $^{10}\text{Be}_{\text{met}}$  deposition rates from contemporary measurements of  $^{10}\text{Be}_{\text{met}}$  in precipitation, corrected for dust and normalized to a modern (1951-2004) solar modulation value (700 MV). A first order estimate of the  $F(^{10}\text{Be}_{\text{met}})$  was empirically derived given  
125 latitude (L) and average precipitation rate (P) to the study area (Graly et al., 2011):

$$F(^{10}\text{Be}_{\text{met}}) = P \times (1.44 / (1 + \text{EXP}((30.7 - L) / 4.36)) + 0.63) \quad (1)$$

Uncertainty for this type of estimate can be determined using the root mean square error ( $1.75 \times 10^3 \text{ atoms cm}^{-3}$ ) of the  
130 resultant latitudinal trend in predicted  $F(^{10}\text{Be}_{\text{met}})$  (see Fig. 5 of Graly et al., 2011). A predicted  $F(^{10}\text{Be}_{\text{met}})$  of  $0.55 (\pm 0.05) \times 10^6$   
atoms  $\text{cm}^{-2} \text{ y}^{-1}$  is calculated for these Wind River moraines using (Eq. 1), however in order to compare these two estimates  
with each other, as well as to our calculated  $F(^{10}\text{Be}_{\text{met}})$ , we later normalize them all to a common paleomagnetic and solar  
intensity datum (i.e. the Holocene).

### 3 Methods

#### 135 3.1 Recalculating Previous Age Constraints

Ages for each moraine have been independently determined via multiple methods, with  $^{10}\text{Be}_{\text{in situ}}$  surface exposure ages of  
boulders combined with  $^{230}\text{Th}/\text{U}$  ages of nearby contemporaneous fluvial terraces yielding the most reliable average  
estimates of 21 ky and 140 ky for the Type-Pinedale and Bull Lake-age moraines, respectively (Gosse et al., 1995; Phillips et  
al., 1997; Easterbrook et al., 2003; Sharp et al., 2003). These ages closely correspond with global maximum ice volumes of  
140 marine oxygen isotope stages 2 and 6, respectively (Sharp et al., 2003). We recalculated the  $^{10}\text{Be}$  boulder surface exposure  
ages used to constrain the timing of advancement of each moraine to its terminal position based on a recent revision of the  
 $^{10}\text{Be}$  half-life, which affected the AMS standard values (Chmeleff et al., 2010), and the most recent nucleonic production rate  
of  $3.92 \text{ atoms g}^{-1} \text{ y}^{-1}$  at sea level-high latitude (Borchers et al., 2016) (Table S1); the updated independent age constraints are  
25 ky for the Pinedale moraine and remain at 140 ky for the Bull Lake moraine (see Supplementary Material for details).

### 145 3.2 Recalculating Previous Denudation Constraints

All moraine surfaces have been eroded to some extent after their deposition. To estimate the amount of erosion for our calculations, we utilize the previously reported denudation rates (comprising erosion and chemical loss by dissolution) for the Pinedale and Bull Lake moraines (Schaller et al., 2009a) from the same depth profiles and material analyzed in this study. The denudation rates of Schaller et al. (2009a) were calculated using a sea level, high latitude production rate of  $5.1 \times 10^{-7}$  atoms  $g_{(qtz)}^{-1} y^{-1}$  (Stone, 2000) and a decay constant of  $4.62 \times 10^{-7} y^{-1}$ . Denudation rates were recalculated using CRONUS v.3 (Phillips et al., 2016) with the updated half-life and production rate values (Table S1) and updated independent age constraints scaled to the sample altitude and latitude (Dunai, 2000) assuming two denudation rate scenarios: one of constant denudation since moraine deposition, and the other of transient denudation decreasing in magnitude since moraine deposition. Recalculated average denudation rates are  $32.1 \pm 2.7$  mm  $ky^{-1}$  and  $12.4 \pm 4.8$  mm  $ky^{-1}$  for the Pinedale and Bull Lake moraines, respectively, in the case of transient denudation, and are 15 mm  $ky^{-1}$  and 7.5 mm  $ky^{-1}$  for the Pinedale and Bull Lake moraines, respectively, in the case of constant denudation (Table 1). These recalculated denudation rates are determined from the best-fit Chi-Square solutions obtained from running Models 2, 4, 6, and 8 of Schaller et al. (2009a) with present-day parameters (See Supplementary Material for details). We consider the transient denudation rates to more closely approximate reality, as moraines, deposited as ~triangular landforms at the terminus of glaciers, initially experience faster denudation than that towards present day, where the moraines evolve to a concave-down parabolic geometry. As the curvature of the topography reduces over time, hillslope diffusion law dictates that the denudation rates will decrease as the moraine flattens. This approach integrates this transient behavior over the entire age of each moraines, and thus likely overstates the loss of  $^{10}Be$  to erosion to some degree, however it nonetheless provides the most realistic estimates possible for these moraines as we are otherwise unable to independently constrain their site-specific erosion rates.

165

To properly compare the transient denudation rates of Schaller et al. (2009a) with the  $^{10}Be_{met}$ -derived erosion rates using the methods of von Blanckenburg et al. (2012), the weathering component of denudation must be accounted for. For the Pinedale moraine, chemical weathering mass loss is estimated to be 16% of the denudation rate, while for the Bull Lake moraine, the chemical weathering mass loss accounts for 20% (Schaller et al., 2009b). Assuming that the weathering mass

170 loss took place beneath the cosmic ray attenuation pathway, the recalculated average effective transient erosion rates are then  
27.0 mm ky<sup>-1</sup> and 9.9 mm ky<sup>-1</sup> for the Pinedale and Bull Lake moraines, respectively. As we have no means to assess  
whether this assumption is correct, we instead account for this degree of potential loss in the uncertainties (in addition to  
analytical uncertainties) on the effective transient erosion rates in all further calculations. Regardless, we note that such  
weathering mass loss does not necessarily need to coincide with loss of dissolved <sup>10</sup>Be<sub>met</sub>. Rather, the sites of primary  
175 mineral dissolution might also be the sites of secondary mineral formation and high dissolved Ca ensuing circumneutral pH  
and hence potentially high <sup>10</sup>Be<sub>met</sub> retentivity.

### 3.3 <sup>10</sup>Be<sub>met</sub> Analysis

We analyzed approximately 1-2 g aliquots of the <2 mm grain-size moraine sediment fraction from the same ~10-15 cm  
depth intervals as Schaller et al. (2009a) analyzed for Be isotope abundance at the Laboratory for the Geochemistry of the  
180 Earth Surface at GFZ Potsdam. We followed the sediment leaching procedure described in Ebert et al. (2012) and Wittmann  
et al. (2012), which was adapted from Bourlés (1988) and Guelke-Stelling and von Blanckenburg (2012), to extract Be  
isotopes from outer grain surfaces. Bulk samples underwent two steps to remove the adsorbed beryllium: a 24-hr agitation in  
0.5 M HCl (to extract amorphous oxide-bound Be), and 1 M hydroxylamine-hydrochloride (to remove crystalline-bound  
Be). After each step, the supernate was separated from the sediment.

185 To measure the adsorbed <sup>10</sup>Be<sub>met</sub>, the two aliquots of leached material were combined and homogenized with ~200 µg of <sup>9</sup>Be  
carrier (Table 2) and 2 mL HF was added to the acid sample solution. This solution was nearly completely dried down and  
then dissolved in 1 additional mL of 50% HF acid and dried down completely, repeated once. We then added 10 mL  
ultrapure (18 MΩ) water to the warm fluoride residue and leached it for 1 h on a warm hotplate. The water containing the Be  
190 was gently removed via pipette and dried down separately. The Be in the water leach solution was extracted and purified by  
a form of the ion exchange chromatography procedure from von Blanckenburg et al. (2004) that was adapted for <sup>10</sup>Be<sub>met</sub>  
purification by passing the leachate through anion (2 ml of BioRad 1x8 100-200 mesh resin) and cation (2x 1 ml BioRad  
AG50-X8 200-400 mesh) exchange resins, precipitated at pH ~9 using NH<sub>4</sub>OH:H<sub>2</sub>O (1:1), washed twice with 2 ml ultrapure  
water with centrifugation in between, mixed with AgCl, centrifuged and dried overnight, and finally oxidized over open



195 flame (>1000 °C; modified from Kohl & Nishiizumi, 1992).  $^{10}\text{Be}_{\text{met}}/^9\text{Be}$  ratios were measured at the Zurich AMS Lab (Kubik and Christl, 2010) (S555 standard, nominal  $^{10}\text{Be}/\text{Be} = 95.5 \times 10^{-12}$ ), from which the  $^{10}\text{Be}$  concentration ( $^{10}\text{Be}_{\text{reac}} = ^{10}\text{Be}_{\text{met}}$ ) was calculated. Two carrier blanks analyzed with the samples register AMS  $^{10}\text{Be}/^9\text{Be}$  ratios of  $3.2 \pm 1.5 \times 10^{-15}$ , and  $2.2 \pm 1.5 \times 10^{-15}$  containing  $\ll 0.1\%$  of the  $^{10}\text{Be}$  in analyzed samples.

### 3.4 $^{10}\text{Be}_{\text{met}}$ Flux Calculations

200 In an actively eroding setting, erosion rates can be calculated with knowledge of 1) the total inventory of  $^{10}\text{Be}_{\text{met}}$  in the depth profile, 2) a known/estimated  $^{10}\text{Be}_{\text{met}}$  flux to the location, 3) the  $^{10}\text{Be}_{\text{met}}$  retention behavior, and 4) an assumption of approximate steady state conditions, which is only justified if the inventory of  $^{10}\text{Be}_{\text{met}}$  is independent of the initial exposure age of the soil. Here, steady state means that  $^{10}\text{Be}_{\text{met}}$  lost through erosion and decay equals the  $^{10}\text{Be}_{\text{met}}$  gained from atmospheric flux (e.g. Brown et al., 1988; Willenbring and von Blanckenburg, 2010), a prerequisite of which is that the residence time of soil material containing  $^{10}\text{Be}_{\text{met}}$  with respect to erosion is much less than the depositional age (Willenbring and von Blanckenburg, 2010), which holds true for these moraines. For an assumed steady state inventory, the inverse relationship between the local erosion rate and the  $^{10}\text{Be}_{\text{met}}$  content in the soil profile is exploited to determine a flux of  $^{10}\text{Be}_{\text{met}}$  using the formulation of Brown (1987), rearranged as follows:

$$210 \quad F(^{10}\text{Be}_{\text{met}}) = E \times ([^{10}\text{Be}]_{\text{reac}} - [^{10}\text{Be}]_{\text{inher}}) + I\lambda \quad (2)$$

Where E is the erosion rate [ $\text{g cm}^{-2} \text{y}^{-1}$ ],  $F(^{10}\text{Be}_{\text{met}})$  is the atmospheric flux of  $^{10}\text{Be}_{\text{met}}$  [ $\text{atoms cm}^{-2} \text{y}^{-1}$ ],  $[^{10}\text{Be}]_{\text{inher}}$  is the inherited nuclide concentration [ $\text{atoms cm}^{-2}$ ], I is the inheritance-corrected inventory of  $^{10}\text{Be}_{\text{met}}$  [ $\text{atoms cm}^{-2}$ ] in the depth profile,  $\lambda$  is the decay constant of  $^{10}\text{Be}$  [ $\text{y}^{-1}$ ],  $[^{10}\text{Be}]_{\text{reac}}$  is the  $^{10}\text{Be}_{\text{met}}$  concentration at the surface of the soil [ $\text{atoms g}^{-1}$ ]. Inventories were calculated following Willenbring and von Blanckenburg (2010) using a depth-averaged regolith density ( $\rho$ ) of  $2.0 \text{ g cm}^{-3}$  for each profile (Schaller et al., 2009a,b), where z is the depth to the bottom of the soil column and  $([^{10}\text{Be}]_{\text{reac}}(z) - [^{10}\text{Be}]_{\text{inher}})$  is the concentration of  $^{10}\text{Be}_{\text{met}}$  at depth, minus inheritance:

$$220 \quad I = \int_0^z ([^{10}\text{Be}]_{\text{reac}}(z) - [^{10}\text{Be}]_{\text{inher}}) \rho dz \quad (3)$$

Both  $^{10}\text{Be}_{\text{met}}$  and  $^{10}\text{Be}_{\text{in situ}}$  depth profiles show indications of inherited nuclide concentrations at depth, likely due to incomplete glacial erosion resetting for each moraine (Schaller et al., 2009a) and exposure to  $^{10}\text{Be}_{\text{met}}$  during or immediately after glacial processes. Higher concentrations at depth are observed for the Bull Lake moraine for both nuclide profiles (Fig. 225 1, Table 2), potentially due to the presence of pre-irradiated reworked till. We consider the lowest concentration observed for each depth profile as  $[^{10}\text{Be}]_{\text{inher}}$  and subtract it from all measured concentrations.

Desorption of  $^{10}\text{Be}_{\text{met}}$  can affect the inventory of  $^{10}\text{Be}_{\text{met}}$  when erosion rates are low, water flux is high and soil chemistry favors mobility. Given that for these soil profiles pH ranges from 8 at depth to  $\sim 5.5$  at the surface (Hall and Shroba, 1995), 230 we must consider incomplete retention of beryllium and thus a reduced inventory and surface concentration used in (Eq. 2) (Bacon et al., 2012; Maher and von Blanckenburg, 2016). Applying a correction directly to the calculation of  $^{10}\text{Be}_{\text{met}}$  flux is possible via a combination of (Eq. 2) (this study) and (Eq. 3) of von Blanckenburg et al. (2012), which requires an accurate estimation of the water flux out of the system (Q) and the Be partition coefficient ( $K_d$ ).

$$235 \quad F(^{10}\text{Be}_{\text{met}}) = E \times ([^{10}\text{Be}]_{\text{reac}} - [^{10}\text{Be}]_{\text{inher}}) + I\lambda + Q \times ([^{10}\text{Be}]_{\text{reac}} - [^{10}\text{Be}]_{\text{inher}}) \div K_d \quad (4)$$

$K_d$  is estimated as  $1 \times 10^5$  to  $1 \times 10^6$  L kg<sup>-1</sup> (with an average of  $5.5 \times 10^5$  L kg<sup>-1</sup>) from the surficial pH of  $\sim 5.5$  to  $\sim 8$  at depth via Be sorption-desorption experiments from You et al. (1989). We estimate Q by proxy via the modern precipitation rate of 276 L m<sup>-2</sup> y<sup>-1</sup>.

240

Utilizing (Eq. 4) and previous knowledge of the effective transient erosion rates, we calculate the loss-corrected  $F(^{10}\text{Be}_{\text{met}})$  to the locations of these moraines. To further account for the full range of possible  $K_d$  values and transient erosion rates, we use traditional algebraic error propagation to determine the uncertainty of the calculated fluxes.

### 3.6 Normalizing flux estimates for cosmic ray intensity variations over the Holocene

245 Geomagnetic field strength has varied considerably from the late Pleistocene to present and exerts the primary quantifiable influence on temporal variability in the production rate of cosmogenic nuclides in an inverse fashion (Pigati and Lifton, 2004). Relative paleointensity over the last 140 ky is, on average, ~20-40% less than the current geomagnetic intensity depending on the methodology employed (e.g. Frank et al., 1997; Valet et al., 2005). The flux map of Heikkilä and von Blanckenburg (2015) accounts for paleomagnetic field and solar intensity variations over the Holocene via the reconstruction  
250 method of Steinhilber et al. (2012), which effectively increases the production rate used in their model by 1.23 times the present-day rate by rescaling the modern solar modulation factor (500 MV) and associated geomagnetic field intensity to that of the Holocene average (280.94 MV). As the estimations of flux from Graly et al. (2011) were normalized to reflect a solar modulation of 700 MV, we rescaled the modern Graly-derived  $F_{(^{10}\text{Be}_{\text{met}})}$  to the average Holocene solar modulation factor of 280.94 MV used in the flux map of Heikkilä and von Blanckenburg (2015) following the paleomagnetic and solar intensity  
255 normalization procedure of Deng et al. (2020). This is carried out by first rescaling production at 700 MV to 500 MV (i.e. the modern solar modulation factor of Steinhilber et al., 2012) via Fig. 4B of Masarik & Beer (2009) for a Graly et al. (2011)-specific modern production ratio of 0.82 (Table 3). Then, to properly normalize for the Holocene, we multiply this modern production ratio by the reciprocal of the rescaling production ratio of Heikkilä and von Blanckenburg (2015) (1.23) to arrive at a Holocene-normalized production ratio of 0.67 and apply this to the Graly et al. (2011) flux estimate (Table 3).  
260 We illustrate and further describe the details of this procedure in the Supplementary Material (Fig. S1).

To further compare the model- and the precipitation-derived Holocene-average  $F_{(^{10}\text{Be}_{\text{met}})}$  estimates with those calculated in this study, we must also normalize for geomagnetic and solar intensity variations within the Holocene (for Pinedale, with a 6 ky cosmogenic integration time) and beyond the Holocene (for Bull Lake, with a 24 ky cosmogenic integration time). We  
265 again linearly rescaled our calculated loss-corrected  $F_{(^{10}\text{Be}_{\text{met}})}$  for the Pinedale and Bull Lake moraines by first integrating the production rate relative to the modern using the Principle Component 1 (PC1) of the  $^{10}\text{Be}$  marine core record of Christl et al. (2010), converting PC1 into relative fluxes from 6 ky and 24 ky, respectively, and then normalizing these values to those over the Holocene, propagating the statistical uncertainties. These time intervals represent the calculated

residence/integration times of the soil profiles from the surface to the e-folding adsorption depth of  $^{10}\text{Be}_{\text{met}}$  (20 and 30 cm for  
270 the Pinedale and Bull Lake moraines, respectively). This approach accounts for the cumulative effects of transient erosion  
and leaching by weighting geomagnetic intensity variations on  $F(^{10}\text{Be}_{\text{met}})$  towards the present.

## 4 Results

### 4.1 Meteoric Cosmogenic $^{10}\text{Be}$ Concentrations

The measured  $^{10}\text{Be}_{\text{met}}$  concentrations are reported along with the previously published  $^{10}\text{Be}_{\text{in situ}}$  concentrations (Schaller et  
275 al., 2009a) for the Pinedale and Bull Lake profiles (Table 2);  $^{10}\text{Be}_{\text{met}}$  depth profiles are presented for the Pinedale and Bull  
Lake profiles in Figure 2. The Pinedale depth profile has  $^{10}\text{Be}_{\text{met}}$  concentrations ranging from  $3.57 (\pm 0.32)$  to  $199.53 (\pm$   
 $5.26) \times 10^6 \text{ atoms g}^{-1}$ . The highest nuclide concentration is measured at 10 cm, rather than at the surface. Below this  
maximum value, concentrations decrease exponentially until reaching an asymptote at  $\sim 3$  to  $6 \times 10^6 \text{ atoms g}^{-1}$  from 43 cm to  
the bottom of the profile (180 cm), the lowest of which we consider to be an inherited component. The Pinedale depth profile  
280 has a calculated, inheritance-corrected inventory (Eq. 3) of  $5387 (\pm 122) \times 10^6 \text{ atoms cm}^{-2}$ .

The Bull Lake depth profile has  $^{10}\text{Be}_{\text{met}}$  concentrations ranging from  $6.32 (\pm 0.25)$  to  $415.48 (\pm 12.46) \times 10^6 \text{ atoms g}^{-1}$ . The  
highest nuclide concentration is measured at the surface; below this, concentrations decrease in an approximately  
exponential fashion until reaching an asymptote at  $\sim 6$  to  $8 \times 10^6 \text{ atoms g}^{-1}$  from 64 cm to the bottom of the profile (130 cm),  
285 the lowest of which we also consider to be an inherited component. The Bull Lake depth profile has a calculated,  
inheritance-corrected inventory (Eq. 3) of  $17310 (\pm 318) \times 10^6 \text{ atoms cm}^{-2}$ . The  $^{10}\text{Be}_{\text{met}}$  inventory from the Bull Lake moraine  
is roughly 3 times higher than that of the Pinedale moraine.

### 4.2 $^{10}\text{Be}_{\text{met}}$ Fluxes

The loss-corrected  $F(^{10}\text{Be}_{\text{met}})$  as calculated from (Eq. 4) is  $1.04 (\pm 0.14) \times 10^6 \text{ atoms cm}^{-2} \text{ y}^{-1}$  and  $1.04 (\pm 0.39) \times 10^6 \text{ atoms cm}^{-2}$   
290  $\text{y}^{-1}$  for the Pinedale and Bull Lake moraines, respectively (Table 3), with uncertainties determined via traditional algebraic  
error propagation, assuming a Gaussian distribution for the estimated  $K_d$  and transient erosion rate values.

Retention calculations from (Eq. 4) across the entire range of possible  $K_d$  values indicate that the potential desorption loss at the surface of the Pinedale and Bull Lake profiles ranges from 0.4% to 3.6% and 0.9% to 8.9%, respectively. The average  
295 calculated loss (reported above) compared to calculations without considering retention is 0.8% and 2.0% for the Pinedale and Bull Lake profiles, respectively.

These loss-corrected calculated fluxes are then normalized for paleomagnetic field intensity variations over the Holocene and compared in order to evaluate the  $F(^{10}\text{Be}_{\text{met}})$  to this area. The Holocene-average loss-corrected  $F(^{10}\text{Be}_{\text{met}})$  from this study are  
300  $1.46 (\pm 0.20) \times 10^6 \text{ atoms cm}^{-2} \text{ y}^{-1}$  and  $1.30 (\pm 0.48) \times 10^6 \text{ atoms cm}^{-2} \text{ y}^{-1}$  for the Pinedale and Bull Lake moraines, respectively (Table 3).

The predicted Holocene-average  $F(^{10}\text{Be}_{\text{met}})$  of Graly et al. (2011) for this site is  $0.83 (\pm 0.08) \times 10^6 \text{ atoms cm}^{-2} \text{ y}^{-1}$  (Table 3). As the pre-industrial flux map of Heikkilä and von Blanckenburg (2015) already presents a Holocene-average  $F(^{10}\text{Be}_{\text{met}})$  of  
305  $1.38 (+ 0.99) \times 10^6 \text{ atoms cm}^{-2} \text{ y}^{-1}$ , no normalization for this method needs to be carried out.

## 5 Discussion

### 5.1 Cosmogenic Nuclide Profiles

An approximately exponential decrease in  $^{10}\text{Be}_{\text{met}}$  with depth is observed for the Pinedale and Bull Lake moraines (Fig. 2). This trend can be explained most simply by the reactive transport of dissolved  $^{10}\text{Be}_{\text{met}}$  with infiltrating water (e.g.  
310 Willenbring and von Blanckenburg, 2010), as exponential  $^{10}\text{Be}_{\text{met}}$  profiles are predicted by reactive transport models (Maher and von Blanckenburg, 2016).

The maximum  $^{10}\text{Be}_{\text{met}}$  concentration for the Pinedale moraine is measured at 10 cm depth, rather than the most surficial sample (3 cm). This peak concentration corresponds with the clay rich layer of the B-horizon in the soil profile (Table 2).  
315 This potentially indicates that this layer acts as a zone of illuviation, often observed in soil profiles that contain a mid-depth

clay-rich horizon (e.g. Monaghan et al., 1992) formed by vertical transport of soil particles containing  $^{10}\text{Be}_{\text{met}}$  (Jagercikova et al., 2016). This subsurface maximum could be the result of smaller grain sizes within this horizon, as these grains have a higher surface area per unit mass and can exchange ions more easily (Brown et al., 1992; Willenbring and von Blanckenburg, 2010). Alternatively, enhanced  $^{10}\text{Be}_{\text{met}}$  incorporation into the lattices of newly formed clays and oxyhydroxides at depth (e.g. Barg et al., 1997) might explain this maximum. This phenomenon is not observed for the Bull Lake moraine; the highest clay content observed in the profile is in the Bk-horizon at a depth of 43 cm (Schaller et al., 2009a,b), however no increase or anomalous high  $^{10}\text{Be}_{\text{met}}$  concentration is observed (Fig. 2, Table 2). It is possible that such an increase may have been missed in the Bull Lake profile, as the equivalent 10 cm depth interval was not sampled.

Peculiarly, the observed mixing depths for the Pinedale and Bull Lake moraines as determined from the  $^{10}\text{Be}_{\text{in situ}}$  depth profiles of Schaller et al. (2009a) (~40 and 50 cm, respectively) are not observed for the  $^{10}\text{Be}_{\text{met}}$  depth profiles (Fig. 2). A couple of viable reasons for a lack of a mixing signal in the  $^{10}\text{Be}_{\text{met}}$  depth profiles exist. The different grain sizes analyzed here and in Schaller et al. (2009a) might exhibit different diffusion coefficients, by which larger grain sizes are more easily mixed, however a trend in smaller grain size fractions with depth within the  $^{10}\text{Be}_{\text{in situ}}$  mixing layer would likely be observed if this were the case. Unfortunately, separate grain size classes were not measured for  $^{10}\text{Be}_{\text{in situ}}$  within the full mixing zone of either profile to further assess this explanation. Another possibility is that the advection of  $^{10}\text{Be}_{\text{met}}$  from the surface swamps the effect of mixing that is apparent in the  $^{10}\text{Be}_{\text{in situ}}$  depth profiles. This could indicate that continual  $^{10}\text{Be}_{\text{met}}$  delivery and reactive flow resets the  $^{10}\text{Be}_{\text{met}}$  profile at timescales much shorter than that of physical mixing. Profiles with a relatively low surficial pH (<5) might be particularly susceptible to this phenomenon due to incomplete retention or differential mobility of  $^{10}\text{Be}_{\text{met}}$  (Kaste and Baskaran, 2011), although the profiles analyzed here are not likely to show appreciable (>9%)  $^{10}\text{Be}_{\text{met}}$  loss at depth due to retention issues. Nonetheless, the formation of a clay horizon in the Pinedale moraine may indicate that soil horizonation happens more rapidly than soil mixing, as inferred from the  $^{10}\text{Be}_{\text{in situ}}$  depth profile (Schaller et al., 2009a), suggesting that  $^{10}\text{Be}_{\text{met}}$  advection from the surface is a more likely explanation.

### 5.1.1 $^{10}\text{Be}_{\text{met}}$ Retention

340 A range of possibilities exist for retention effects and associated surficial  $^{10}\text{Be}_{\text{met}}$  loss for these profiles. For the highest  $K_d$  estimate, at  $1 \times 10^6 \text{ L kg}^{-1}$ , potential loss is as low as 0.4% and 0.8% for the Pinedale and Bull Lake profiles, respectively. For an average  $K_d$  of  $5.5 \times 10^5 \text{ L kg}^{-1}$ , the potential loss is likewise negligible, at 0.8% and 2.0% for the Pinedale and Bull Lake profiles, respectively. On the other hand, for the lowest  $K_d$  estimate, at  $1 \times 10^5 \text{ L kg}^{-1}$ ,  $^{10}\text{Be}_{\text{met}}$  loss due to desorption could be as great as 3.6% and 8.9% at the surface of the Pinedale and Bull Lake profiles, respectively. While the possibility  
345 of desorption cannot be ruled out, it's unlikely that either profile has experienced loss to such a degree, as pH, and thus  $K_d$  and retentivity, increases with depth. Even in the worst-case scenario of assuming maximum possible loss at the lowest  $K_d$  estimate, the magnitude of the potential loss does not substantially affect our calculated  $F(^{10}\text{Be}_{\text{met}})$  estimates within uncertainties. Our calculations thus capture the potential maximum bound for loss via propagated uncertainties.

### 5.2 $^{10}\text{Be}_{\text{met}}$ flux estimation; sources of variability

350 The calculated, loss- and paleointensity-corrected  $F(^{10}\text{Be}_{\text{met}})$  of  $1.46 (\pm 0.20) \times 10^6 \text{ atoms cm}^{-2} \text{ y}^{-1}$  and  $1.30 (\pm 0.48) \times 10^6 \text{ atoms cm}^{-2} \text{ y}^{-1}$  for the Pinedale and Bull Lake moraines, respectively, are higher compared to that estimated by Graly et al. (2011), at  $0.83 \times 10^6 \text{ atoms cm}^{-2} \text{ y}^{-1}$ , and agree within uncertainty with that predicted by Heikkilä and von Blanckenburg (2015), at  $1.38 \times 10^6 \text{ atoms cm}^{-2} \text{ y}^{-1}$  (Table 3). The considerable discrepancy between the predicted  $F(^{10}\text{Be}_{\text{met}})$  of each method arises primarily from differences in how each methodology treats the influence that precipitation rate has on the flux to a  
355 given area and, in particular for this study, how large of an area is covered. The  $310 \text{ km} \times 228 \text{ km}$  flux map grid cell of Heikkilä and von Blanckenburg (2015) covers the entirety of the Wind River Range and the surrounding, relatively low-lying flatlands (Fig. 1), where precipitation estimates vary considerably, by over an order of magnitude (WRCC, 2005), due to elevation and topographic effects on precipitation (Hostetler and Clark, 1997). For example, if one were to estimate  $F(^{10}\text{Be}_{\text{met}})$  from Graly et al. (2011) via (Eq. 1) to nearby Fish Lake Mountain contained within the same Heikkilä and von  
360 Blanckenburg (2015) grid cell as this study site, with a modern precipitation rate of  $128 \text{ cm y}^{-1}$  (WRCC, 2005), the  $F(^{10}\text{Be}_{\text{met}})$  would be  $2.5 \times 10^6 \text{ atoms cm}^{-2} \text{ y}^{-1}$ , substantially higher than that predicted from Heikkilä and von Blanckenburg (2015).

Considering this alone, it is not surprising that such a discrepancy exists between methods, nor is this a unique occurrence (e.g. Jungers et al., 2009; Schoonejans et al., 2017; Dixon et al., 2018; Deng et al., 2020).

365 Each approach has its own set of shortcomings, precluding agreement between each approach in sites such as this. The flux map of Heikkilä and von Blanckenburg (2015) has a coarse resolution and does not handle short wavelength orographic effects well, along with being model based and requiring many assumptions on atmospheric scavenging. The formula of Graly et al. (2011), on the other hand, does not take atmospheric circulation into account, instead relying on data from sites with relatively high rates of precipitation to derive an empirical formula. Recent work by Deng et al. (2020) highlights the  
370 potential for precipitation estimates to differ from GCM-derived estimates due to short timescale additive effects (*sensu* Willenbring and von Blanckenburg, 2010). Further, they find that in the majority of studies globally, GCM- and soil-derived  $F(^{10}\text{Be}_{\text{met}})$  estimates agree within a factor of two. That the calculated fluxes of this study agree with the GCM-modeled pre-industrial  $F(^{10}\text{Be}_{\text{met}})$  of Heikkilä and von Blanckenburg (2015) provides further evidence of this general observation. In any event, the strength of future  $^{10}\text{Be}_{\text{met}}$  studies relies upon careful consideration of beryllium retention, spatial scale, and  
375 paleomagnetic intensity when determining  $F(^{10}\text{Be}_{\text{met}})$ . As calculating a long-term delivery rate of  $F(^{10}\text{Be}_{\text{met}})$  for a particular site using  $^{10}\text{Be}_{\text{in situ}}$  and  $^{10}\text{Be}_{\text{met}}$  is both costly and time-intensive, it is especially prudent to estimate  $F(^{10}\text{Be}_{\text{met}})$  using both methods compared here for robust calculations utilizing  $F(^{10}\text{Be}_{\text{met}})$  (e.g.  $^{10}\text{Be}_{\text{met}}$ -derived erosion rates) in the future.

## 6. Conclusions

In this study, we compare new meteoric  $^{10}\text{Be}$  ( $^{10}\text{Be}_{\text{met}}$ ) and previously published *in situ*-produced  $^{10}\text{Be}$  ( $^{10}\text{Be}_{\text{in situ}}$ ) depth  
380 profile measurements from the well-characterized Pinedale (~21-25 ky) and Bull Lake (~140 ky) moraines of Wind River, Wyoming. Our ability to utilize previous knowledge of transient erosion rates from the  $^{10}\text{Be}_{\text{in situ}}$  depth profile measurements of Schaller et al. (2009a), recalculated with revised parameters, allows us to calculate loss-corrected Holocene average  $^{10}\text{Be}_{\text{met}}$  fluxes of  $1.46 (\pm 0.20) \times 10^6$  atoms  $\text{cm}^{-2} \text{y}^{-1}$  and  $1.30 (\pm 0.48) \times 10^6$  atoms  $\text{cm}^{-2} \text{y}^{-1}$  to the Pinedale and Bull Lake moraines, respectively. Comparing these fluxes to two independent estimation methods reveals that the empirical flux



385 estimate of Graly et al. (2011), after normalizing for Holocene paleomagnetic intensity, at  $0.83 (\pm 0.08) \times 10^6$  atoms  $\text{cm}^{-2} \text{y}^{-1}$ ,  
is lower than the calculated fluxes, and the modeled Holocene flux estimate of Heikkila and von Blanckenburg (2015), at  
 $1.38 \times 10^6$  atoms  $\text{cm}^{-2} \text{y}^{-1}$ , agrees within uncertainty to the calculated fluxes. We find that loss of  $^{10}\text{Be}_{\text{met}}$  in these profiles due  
to pH-influenced mobility/dissolution effects exerts a relatively minor potential control (biasing from <1% up to 9% in the  
most extreme case) on flux calculations. Inspection of the  $^{10}\text{Be}_{\text{met}}$  depth profiles and their near-surface concentrations suggest  
390 that soil mixing to depths of 40 and 50 cm, as observed for the Pinedale and Bull Lake  $^{10}\text{Be}_{\text{in situ}}$  depth profiles, respectively,  
is not represented by the finer grain sizes analyzed in this study. The lack of a mixing signal may be most simply explained  
by a swamping effect from continual delivery and advection of  $^{10}\text{Be}_{\text{met}}$  from the surface that occurs over more rapid  
timescales than soil mixing. These differences in the depth-concentration relationships between  $^{10}\text{Be}_{\text{met}}$  and  $^{10}\text{Be}_{\text{in situ}}$  might  
open up a new area of research to study particle movement in soils.

#### 395 **Author Contribution**

TC is a current Ph.D. student at Stanford University and conducted the majority of the work during 2018-2019 under the  
supervision of JWK, who contributed to several drafts of the original manuscript as well as preparation of the meteoric data  
set at GFZ Potsdam. MS and JDB contributed via  $^{10}\text{Be}$  data acquisition, interpretation, and discussion; MC and PWK  
contributed via AMS measurements at ETH-Zurich. FvB assisted in interpretation of the comparative data set and associated  
400 discussion of meteoric  $^{10}\text{Be}$  flux estimates, mobility/retention, and paleomagnetic field intensity normalization and  
contributed to manuscript drafts.

#### **Competing Interests**

The authors declare no competing interests for this manuscript.

#### **Acknowledgement**

405 This work was made possible through the German Science Foundation Grant *BL562/7* and an Alexander von Humboldt  
Postdoctoral Fellowship. Support for TC came from a Career grant to Willenbring from NSF #1651243. The authors thank  
three anonymous reviewers for constructive comments and suggestions which greatly improved the manuscript.

## References

- 410 Bacon, A. R., Richter, D. D., Bierman, P. R., and Rood, D. H.: Coupling meteoric  $^{10}\text{Be}$  with pedogenic losses of  $^9\text{Be}$  to improve soil residence time estimates on an ancient North American interfluvium, *Geology*, 40(9), 847-850, <https://doi.org/10.1130/G33449.1>, 2012
- 415 Barg, E., Lal, D., Pavich, M. J., Caffee, M. W., and Southon, J. R.: Beryllium geochemistry in soils; evaluation of  $^{10}\text{Be}/^9\text{Be}$  ratios in authigenic minerals as a basis for age models. *Chemical Geology*, 140, 237-258, [https://doi.org/10.1016/S0009-2541\(97\)00051-X](https://doi.org/10.1016/S0009-2541(97)00051-X), 1997.
- Blum, J. D., and Erel, Y.: Rb/Sr isotope systematics of a granitic soil chronosequence: The importance of biotite weathering, *Geochimica et Cosmochimica Acta*, 61(15), 3193-3204, [https://doi.org/10.1016/S0016-7037\(97\)00148-8](https://doi.org/10.1016/S0016-7037(97)00148-8), 1997.
- 420 Borchers, B., Marrero, S., Balco, G., Caffee, M., Goehring, B., Lifton, N., ... and Stone, J.: Geological calibration of spallation production rates in the CRONUS-Earth project, *Quaternary Geochronology*, 31, 188-198, <https://doi.org/10.1016/j.quageo.2015.01.009>, 2016.
- 425 Bourlès, D.: Étude de la géochimie de l'isotope cosmogénique  $^{10}\text{Be}$  et de son isotope stable  $^9\text{Be}$  en milieu océanique: application à la datation des sédiments marins, Ph.D. thesis, Université Paris XI, Centre d'Orsay, 1988.
- Boschi, V., Willenbring, J.K.: The role of pH, organic matter composition and mineralogy on the sorption behavior of beryllium. *Environmental Chemistry*. <http://dx.doi.org/10.1071/EN15107>, 2016a.
- 430 Boschi, V., Willenbring, J.K.: Beryllium Desorption from Minerals and Organic Ligands Over Time. *Chemical Geology*, 439(7) 52–58. <http://dx.doi.org/10.1016/j.chemgeo.2016.06.009>, 2016b.
- Brown, L.:  $^{10}\text{Be}$  as a tracer of erosion and sediment transport. *Chemical Geology: Isotope Geoscience section*, 65(3-4), 189-196, [https://doi.org/10.1016/0168-9622\(87\)90002-9](https://doi.org/10.1016/0168-9622(87)90002-9), 1987.
- 435 Brown, L., Pavich, M. J., Hickman, R. E., Klein, J., Middleton, R.: Erosion of the Eastern United States observed with  $^{10}\text{Be}$ . *Earth Surface Processes and Landforms*, 13, 441-457, <https://doi.org/10.1002/esp.3290130509>, 1988.
- 440 Brown, E. T., Edmond, J. M., Raisbeck, G. M., Bourlès, D. L., Yiou, F., and Measures, C. I.: Beryllium isotope geochemistry in tropical river basins, *Geochimica et Cosmochimica Acta*, 56(4), 1607-1624, [https://doi.org/10.1016/0016-7037\(92\)90228-B](https://doi.org/10.1016/0016-7037(92)90228-B), 1992.
- 445 Chadwick, O. A., & Chorover, J., The chemistry of pedogenic thresholds, *Geoderma*, 100(3-4), 321-353, [https://doi.org/10.1016/S0016-7061\(01\)00027-1](https://doi.org/10.1016/S0016-7061(01)00027-1), 2001.
- Chmeleff, J., von Blanckenburg, F., Kosser, K., and Jakob, D.: Determination of the  $^{10}\text{Be}$  half-life by multicollector ICP-MS and liquid scintillation counting, *Nuclear Instruments and Methods in Physics Research Section B: Beam Interactions with Materials and Atoms*, 268(2), 192–199, <https://doi.org/10.1016/j.nimb.2009.09.012>, 2010.
- 450 Christl, M., Lippold, J., Steinhilber, F., Bernsdorff, F., and Mangini, A.: Reconstruction of global  $^{10}\text{Be}$  production over the past 250 ka from highly accumulating Atlantic drift sediments, *Quaternary Science Reviews*, 29(19-20), 2663-2672, <https://doi.org/10.1016/j.quascirev.2010.06.017>, 2010.
- 455 Deng, K., Wittmann, H., and von Blanckenburg, F.: The depositional flux of meteoric cosmogenic  $^{10}\text{Be}$  from modelling and observation, *Earth and Planetary Science Letters*, 550, 116530, <https://doi.org/10.1016/j.epsl.2020.116530>, 2020.

- Dixon, J. L., Chadwick, O. A., and Pavich, M. J.: Climatically controlled delivery and retention of meteoric  $^{10}\text{Be}$  in soils, *Geology*, 46(10), 899-902, <https://doi.org/10.1130/G45176.1>, 2018.
- 460 Dunai, T. J.: Scaling factors for production rates of in situ produced cosmogenic nuclides: a critical reevaluation, *Earth and Planetary Science Letters*, 176(1), 157-169, [https://doi.org/10.1016/S0012-821X\(99\)00310-6](https://doi.org/10.1016/S0012-821X(99)00310-6), 2000.
- Easterbrook, D. J., Pierce, K., Gosse, J., Gillespie, A., Evenson, E., and Hamblin, K.: Quaternary geology of the western United States, in: *Quaternary Geology of the United States*, edited by: Easterbrook, D. J., Desert Res. Inst., Reno, Nev., 19-79, 2003.
- 465 Ebert, K., Willenbring, J., Norton, K. P., Hall, A., and Hättstrand, C.: Meteoric  $^{10}\text{Be}$  concentrations from saprolite and till in northern Sweden: Implications for glacial erosion and age, *Quaternary Geochronology*, 12, 11-22, <https://doi.org/10.1016/j.quageo.2012.05.005>, 2012.
- 470 Field, C. V., Schmidt, G. A., Koch, D., and Salyk, C.: Modeling production and climate-related impacts on  $^{10}\text{Be}$  concentration in ice cores, *Journal of Geophysical Research: Atmospheres*, 111(D15), <https://doi.org/10.1029/2005JD006410>, 2006.
- 475 Frank, M., Schwarz, B., Baumann, S., Kubik, P. W., Suter, M., and Mangini, A.: A 200 kyr record of cosmogenic radionuclide production rate and geomagnetic field intensity from  $^{10}\text{Be}$  in globally stacked deep-sea sediments, *Earth and Planetary Science Letters*, 149(1-4), 121-129, [https://doi.org/10.1016/S0012-821X\(97\)00070-8](https://doi.org/10.1016/S0012-821X(97)00070-8), 1997.
- Guelke-Stelling, M., and von Blanckenburg, F.: Fe isotope fractionation caused by translocation of iron during growth of bean and oat as models of strategy I and II plants, *Plant and soil*, 352(1-2), 217-231, <https://doi.org/10.1007/s11104-011-0990-9>, 2012.
- 480 Gosse, J. C., Klein, J., Lawn, B., Middleton, R., and Evenson, E. B.: Beryllium-10 dating of the duration and retreat of the last Pinedale glacial sequence, *Science*, 268(5215), 1329-1333, <https://doi.org/10.1126/science.268.5215.1329>, 1995.
- 485 Graly, J. A., Bierman, P. R., Reusser, L. J., and Pavich, M. J.: Meteoric  $^{10}\text{Be}$  in soil profiles—a global meta-analysis, *Geochimica et Cosmochimica Acta*, 74(23), 6814-6892, <https://doi.org/10.1016/j.gca.2010.08.036>, 2010.
- 490 Graly, J. A., Reusser, L. J., and Bierman, P. R.: Short and long-term delivery rates of meteoric  $^{10}\text{Be}$  to terrestrial soils, *Earth and Planetary Science Letters*, 302(3-4), 329-336, <https://doi.org/10.1016/j.epsl.2010.12.020>, 2011.
- Hall, R. D., and Shroba, R. R.: Soil evidence for a glaciation intermediate between the Bull Lake and Pinedale glaciations at Fremont Lake, Wind River Range, Wyoming, USA, *Arctic and Alpine Research*, 27(1), 89-98, <https://doi.org/10.2307/1552071>, 1995.
- 495 Heikkilä, U. and Smith, A. M.: Influence of model resolution on the atmospheric transport of  $^{10}\text{Be}$ , *Atmospheric Chemistry and Physics*, 12(21), 10601-10612, <https://doi.org/10.5194/acp-12-10601-2012>, 2012.
- 500 Heikkilä, U. and Von Blanckenburg, F.: The global distribution of Holocene meteoric  $^{10}\text{Be}$  fluxes from atmospheric models, *GFZ Data Services*, GFZ Potsdam, Germany, <http://doi.org/10.5880/GFZ.3.4.2015.001>, 2015.
- Hostetler, S. W., and Clark, P. U.: Climatic controls of western US glaciers at the last glacial maximum, *Quaternary Science Reviews*, 16(6), 505-511, [https://doi.org/10.1016/S0277-3791\(96\)00116-3](https://doi.org/10.1016/S0277-3791(96)00116-3), 1997.

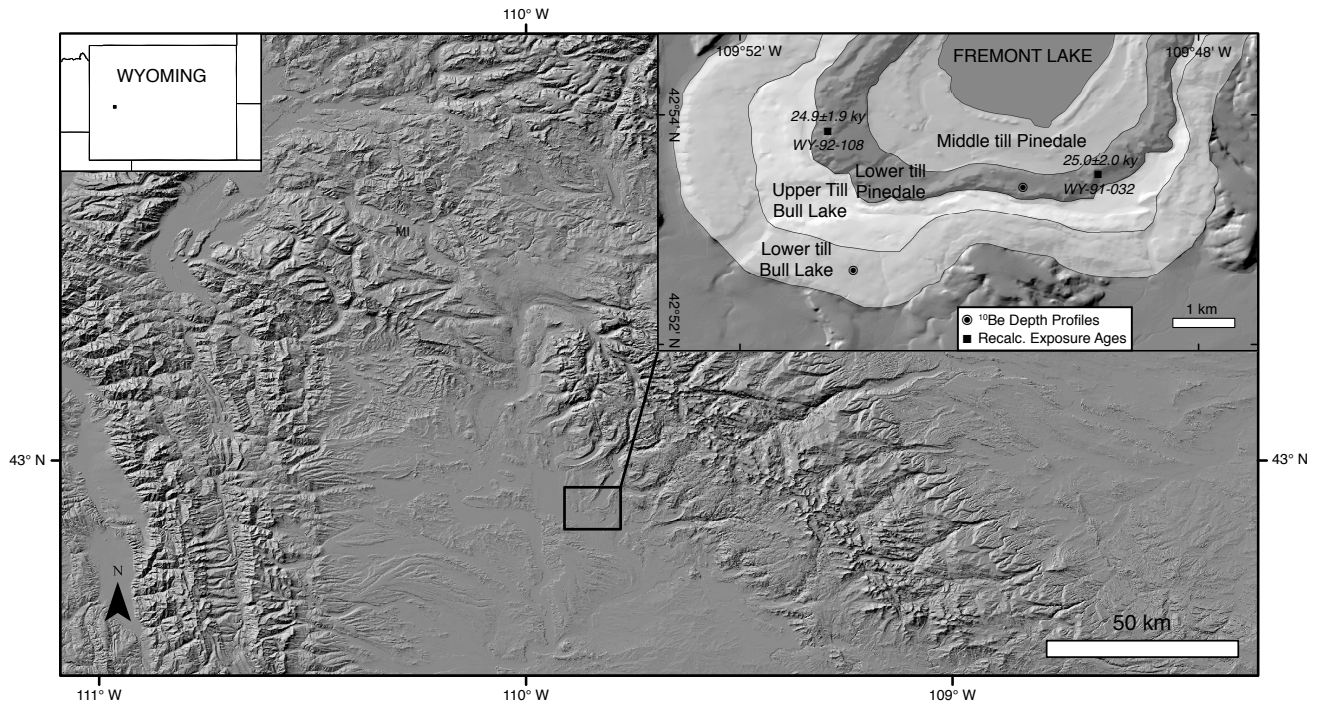
- 505 Jagercikova, M., Cornu, S., Bourlès, D., Evrard, O., Hatté, C. and Balesdent, J.: Quantification of vertical solid matter transfers in soils during pedogenesis by a multi-tracer approach, *Journal of Soils and Sediments*, 17, 408-422, <https://doi.org/10.1007/s11368-016-1560-9>, 2016.
- 510 Jelinski, N., Willenbring, J.K., Schumacher, T.E., Li, S. Lobb, D.A., Papiernik, S.K., and Yoo, K.: Meteoric Beryllium-10 as a tracer of cumulative erosion due to post-settlement land use in west-central Minnesota, USA, *Journal of Geophysical Research – Earth Surface*, 124(4), 874-901, <https://doi.org/10.1029/2018JF004720>, 2019.
- 515 Jungers, M. C., Bierman, P. R., Matmon, A., Nichols, K., Larsen, J., and Finkel, R.: Tracing hillslope sediment production and transport with in situ and meteoric  $^{10}\text{Be}$ , *Journal of Geophysical Research: Earth Surface*, 114(F4), <https://doi.org/10.1029/2008JF001086>, 2009.
- 520 Kaste, J. M., and Baskaran, M.: Meteoric  $^7\text{Be}$  and  $^{10}\text{Be}$  as process tracers in the environment, in: *Handbook of environmental isotope geochemistry*, edited by: Baskaran, M., Springer, Berlin, Heidelberg, 61-85, [https://doi.org/10.1007/978-3-642-10637-8\\_5](https://doi.org/10.1007/978-3-642-10637-8_5), 2012.
- 525 Kubik, P. W., and Christl, M.:  $^{10}\text{Be}$  and  $^{26}\text{Al}$  measurements at the Zurich 6 MV Tandem AMS facility, *Nuclear Instruments and Methods in Physics Research Section B: Beam Interactions with Materials and Atoms*, 268(7-8), 880-883, <https://doi.org/10.1016/j.nimb.2009.10.054>, 2010.
- 530 Kohl, C. P., and Nishiizumi, K.: Chemical isolation of quartz for measurement of in-situ -produced cosmogenic nuclides, *Geochimica et Cosmochimica Acta*, 56(9), 3583-3587, [https://doi.org/10.1016/0016-7037\(92\)90401-4](https://doi.org/10.1016/0016-7037(92)90401-4), 1992.
- 535 Lal, D. and Peters, B.: Cosmic ray produced radioactivity on the Earth, in: *Kosmische Strahlung II/Cosmic Rays II*, edited by: Sitte, K., Springer, Berlin, Heidelberg, 551-612, [https://doi.org/10.1007/978-3-642-46079-1\\_7](https://doi.org/10.1007/978-3-642-46079-1_7), 1967.
- 540 Mahaney, W. C., and Halvorson, D. L.: Rates of mineral weathering in the Wind River Mountains, western Wyoming, in: *Rates of chemical weathering of rocks and minerals*, edited by: Colman, S., and Dethier, D., Academic Press, Cambridge, Massachusetts, 147-167, 1986.
- 545 Maher, K., and von Blanckenburg, F.: Surface ages and weathering rates from  $^{10}\text{Be}$  (meteoric) and  $^{10}\text{Be}/^9\text{Be}$ : insights from differential mass balance and reactive transport modeling, *Chemical Geology*, 446, 70-86, <https://doi.org/10.1016/j.chemgeo.2016.07.016>, 2016.
- 540 Masarik, J., and Beer, J.: Simulation of particle fluxes and cosmogenic nuclide production in the Earth's atmosphere, *Journal of Geophysical Research: Atmospheres*, 104(D10), 12099-12111, <https://doi.org/10.1029/1998JD200091>, 1999.
- 545 Masarik, J., and Beer, J.: An updated simulation of particle fluxes and cosmogenic nuclide production in the Earth's atmosphere, *Journal of Geophysical Research: Atmospheres*, 114(D11), <https://doi.org/10.1029/2008JD010557>, 2009.
- 545 Mckean, J.A., Dietrich, W.E., Finkel, R.C., Southon, J.R., and Caffee, M.W.: Quantification of Soil Production and Downslope Creep Rates from Cosmogenic  $^{10}\text{Be}$  Accumulations on a Hillslope Profile, *Geology*, 21, 343-346, [https://doi.org/10.1130/0091-7613\(1993\)021<0343:QOSPAD>2.3.CO;2](https://doi.org/10.1130/0091-7613(1993)021<0343:QOSPAD>2.3.CO;2), 1993.
- 550 Monaghan, M. C., McKean, J., Dietrich, W., and Klein, J.:  $^{10}\text{Be}$  chronometry of bedrock-to-soil conversion rates, *Earth and Planetary Science Letters*, 111(2-4), 483-492, [https://doi.org/10.1016/0012-821X\(92\)90198-5](https://doi.org/10.1016/0012-821X(92)90198-5), 1992.

- 555 Ouimet, W., Dethier, D., Bierman, P., Wyshnytzkyr, C., Shea, N., and Rood, D. H.: Spatial and temporal variations in meteoric  $^{10}\text{Be}$  inventories and long-term deposition rates, Colorado Front Range, *Quaternary Science Reviews*, 109, 1-12, <https://doi.org/10.1016/j.catena.2014.12.008>, 2015.
- Pavich, M. J., Brown, L., Harden, J., Klein, J., and Middleton, R.:  $^{10}\text{Be}$  distribution in soils from Merced River terraces, California, *Geochimica et Cosmochimica Acta*, 50(8), 1727-1735, [https://doi.org/10.1016/0016-7037\(86\)90134-1](https://doi.org/10.1016/0016-7037(86)90134-1), 1986.
- 560 Phillips, F. M., Zreda, M. G., Gosse, J. C., Klein, J., Evenson, E. B., Hall, R. D., Chadwick, O.A., and Sharma, P.: Cosmogenic  $^{36}\text{Cl}$  and  $^{10}\text{Be}$  ages of Quaternary glacial and fluvial deposits of the Wind River Range, Wyoming, *Geological Society of America Bulletin*, 109(11), 1453-1463, [https://doi.org/10.1130/0016-7606\(1997\)109<1453:CCABAO>2.3.CO;2](https://doi.org/10.1130/0016-7606(1997)109<1453:CCABAO>2.3.CO;2), 1997.
- 565 Phillips, F. M., Argento, D. C., Balco, G., Caffee, M. W., Clem, J., Dunai, T. J., ... and Jull, A. T.: The CRONUS-Earth project: a synthesis, *Quaternary Geochronology*, 31, 119-154, <https://doi.org/10.1016/j.quageo.2015.09.006>, 2016.
- 570 Pigati, J. S. and Lifton, N. A.: Geomagnetic effects on time-integrated cosmogenic nuclide production with emphasis on in situ  $^{14}\text{C}$  and  $^{10}\text{Be}$ , *Earth and Planetary Science Letters*, 226(1-2), 193-205, <https://doi.org/10.1016/j.epsl.2004.07.031>, 2004.
- Portenga, E.W., Bierman, P.R., Trodick Jr, C.D., Greene, S.E., DeJong, B.D., Rood, D.H., and Pavich, M.J.: Erosion rates and sediment flux within the Potomac River basin quantified over millennial timescales using beryllium isotopes, *GSA Bulletin*, 131(7-8), 1295-1311, <https://doi.org/10.1130/B31840.1>, 2019.
- 575 Reusser, L., Graly, J., Bierman, P., and Rood, D.: Calibrating a long-term meteoric  $^{10}\text{Be}$  accumulation rate in soil, *Geophysical Research Letters*, 37(19), <https://doi.org/10.1029/2010GL044751>, 2010.
- Richmond, G. M.: Geologic map of the Fremont Lake south quadrangle, Sublette County, Wyoming, Map 1138, <https://doi.org/10.3133/gq1138>, 1973.
- 580 Schaller, M., Ehlers, T. A., Blum, J. D., and Kyrrlenberg, M. A.: Quantifying glacial moraine age, denudation, and soil mixing with cosmogenic nuclide depth profiles, *Journal of Geophysical Research: Earth Surface*, 114(F1), <https://doi.org/10.1029/2007JF000921>, 2009a.
- 585 Schaller, M., Blum, J. D., & Ehlers, T. A.: Combining cosmogenic nuclides and major elements from moraine soil profiles to improve weathering rate estimates, *Geomorphology*, 106(3-4), 198-205, <https://doi.org/10.1016/j.geomorph.2008.10.014>, 2009b.
- 590 Schoonejans, J., Vanacker, V., Opfergelt, S., and Christl, M.: Long-term soil erosion derived from in-situ  $^{10}\text{Be}$  and inventories of meteoric  $^{10}\text{Be}$  in deeply weathered soils in southern Brazil. *Chemical Geology*, 466, 380-388, <https://doi.org/10.1016/j.chemgeo.2017.06.025>, 2017.
- 595 Sharp, W. D., Ludwig, K. R., Chadwick, O. A., Amundson, R., and Glaser, L. L.: Dating fluvial terraces by  $^{230}\text{Th}/\text{U}$  on pedogenic carbonate, Wind River Basin, Wyoming, *Quaternary Research*, 59(2), 139-150, [https://doi.org/10.1016/S0033-5894\(03\)00003-6](https://doi.org/10.1016/S0033-5894(03)00003-6), 2003.
- 600 Steinhilber, F., Abreu, J. A., Beer, J., and McCracken, K. G.: Interplanetary magnetic field during the past 9300 years inferred from cosmogenic radionuclides, *Journal of Geophysical Research: Space Physics*, 115(A1), <https://doi.org/10.1029/2009JA014193>, 2010.
- Stone, J. O.: Air pressure and cosmogenic isotope production, *Journal of Geophysical Research: Solid Earth*, 105(B10), 23753-23759, <https://doi.org/10.1029/2000JB900181>, 2000.

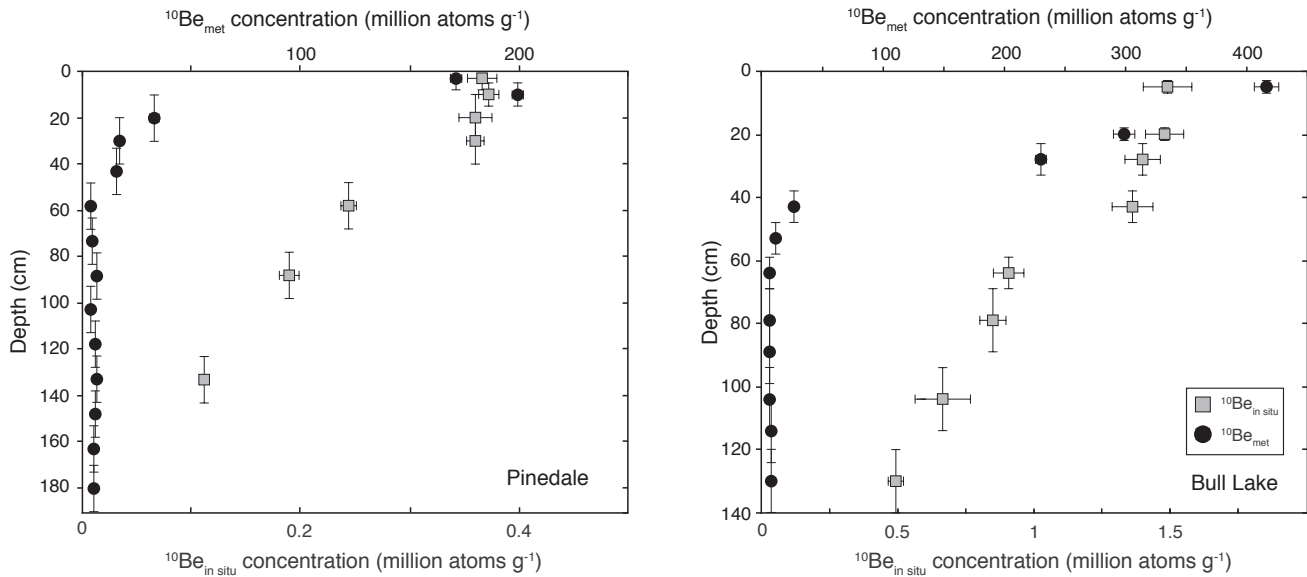
- 605 Taylor, A. and Blum, J. D.: Relation between soil age and silicate weathering rates determined from the chemical evolution of a glacial chronosequence, *Geology*, 23(11), 979-982, [https://doi.org/10.1130/0091-7613\(1995\)023<0979:RBSAAS>2.3.CO;2](https://doi.org/10.1130/0091-7613(1995)023<0979:RBSAAS>2.3.CO;2), 1995.
- 610 Taylor, A. and Blum, J. D.: Relation between soil age and silicate weathering rates determined from the chemical evolution of a glacial chronosequence: Reply, *Geology*, 25(4), 382-383, 1997.
- Valet, J. P., Meynadier, L., and Guyodo, Y.: Geomagnetic dipole strength and reversal rate over the past two million years, *Nature*, 435(7043), 802-805, <https://doi.org/10.1038/nature03674>, 2005.
- 615 von Blanckenburg, F., Hewawasam, T., and Kubik, P. W.: Cosmogenic nuclide evidence for low weathering and denudation in the wet, tropical highlands of Sri Lanka, *Journal of Geophysical Research: Earth Surface*, 109(F3), <https://doi.org/10.1029/2003JF000049>, 2004.
- 620 von Blanckenburg, F., Bouchez, J., and Wittmann, H.: Earth surface erosion and weathering from the  $^{10}\text{Be}$  (meteoric)/ $^9\text{Be}$  ratio, *Earth and Planetary Science Letters*, 351, 295-305, <https://doi.org/10.1016/j.epsl.2012.07.022>, 2012.
- von Blanckenburg, F., and Bouchez, J.: River fluxes to the sea from the ocean's  $^{10}\text{Be}/^9\text{Be}$  ratio. *Earth and Planetary Science Letters*, 387, 34-43, <https://doi.org/10.1016/j.epsl.2013.11.004>, 2014.
- 625 von Blanckenburg, F., Bouchez, J., Ibarra, D.E., and Maher, K.: Stable runoff and weathering fluxes into the oceans over Quaternary climate cycles, *Nature Geoscience*, 8, 538-U146, <https://doi.org/10.1038/ngeo2452>, 2015.
- Willenbring, J. K., and von Blanckenburg, F.: Meteoric cosmogenic Beryllium-10 adsorbed to river sediment and soil: Applications for Earth-surface dynamics. *Earth-Science Reviews*, 98(1-2), 105-122, <https://doi.org/10.1016/j.earscirev.2009.10.008>, 2010.
- 630 Wittmann, H., Von Blanckenburg, F., Bouchez, J., Dannhaus, N., Naumann, R., Christl, M., and Gaillardet, J.: The dependence of meteoric  $^{10}\text{Be}$  concentrations on particle size in Amazon River bed sediment and the extraction of reactive  $^{10}\text{Be}/^9\text{Be}$  ratios, *Chemical Geology*, 318, 126-138, <https://doi.org/10.1016/j.chemgeo.2012.04.031>, 2012.
- 635 Western Regional Climate Center (WRCC): <https://wrcc.dri.edu/>, last access: 18 September 2020, 2005.
- You, C. F., Lee, T., and Li, Y. H.: The partition of Be between soil and water. *Chemical Geology*, 77(2), 105-118, [https://doi.org/10.1016/0009-2541\(89\)90136-8](https://doi.org/10.1016/0009-2541(89)90136-8), 1989.

640

## Figures



645 **Fig. 1)** Hillshade map of the Wind River range, derived from a 10 m digital elevation model (DEM); regional map  
encompasses the entirety of the meteoric  $^{10}\text{Be}$  flux map grid cell of Heikkila and von Blanckenburg (2015). Inset (upper left)  
shows location of regional map within Wyoming. Inset (upper right) shows locations of depth profiles analyzed for  
cosmogenic nuclide concentrations from the terminal Pinedale and Bull Lake moraines in the Fremont Lake area (after  
Richmond, 1973 and Schaller et al., 2009a). Also shown are the locations of boulder surface exposure dates for the Pinedale  
650 moraine (WY-92-108 and WY-91-032 of Gosse et al., 1995) that were recalculated using revised parameters (Table S1) to  
establish an updated independent age constraint for this moraine.



655 **Fig. 2** (Left) Depth profile for the Pinedale moraine;  $^{10}\text{Be}_{\text{met}}$  concentrations were measured from the  $<2$  mm grain-size fraction of 14 samples from the same depth profile as analyzed for  $^{10}\text{Be}_{\text{in situ}}$  in Schaller et al. (2009a). (Right) Depth profile for the Bull Lake moraine;  $^{10}\text{Be}_{\text{met}}$  concentrations were also measured from the  $<2$  mm grain-size fraction of 11 samples from the same depth profile as analyzed for  $^{10}\text{Be}_{\text{in situ}}$  in Schaller et al. (2009a). The  $^{10}\text{Be}_{\text{met}}$  concentration at 94 cm was not measured.

660

**Table 1.** Recalculated Chi-Square Solutions for Different Denudation Rate Simulations of Schaller et al. (2009a)<sup>a</sup>

Type of Denudation	Model	Age (ky; <i>fixed parameter</i> )	Average Denudation (mm ky <sup>-1</sup> )	Inherited $^{10}\text{Be}$ concentration (10 <sup>5</sup> at g <sup>-1</sup> )	Mixing Depth (cm)	Diffusivity $k$ (10 <sup>-3</sup> m <sup>2</sup> y <sup>-1</sup> )	Maximum Height (m)	Slope Angle (degrees)
<i>Pinedale moraine (2262 m asl, 42° 53' 26" N, 109° 49' 34" W)</i>								
Constant	2	25	15	0.2	0			
Transient	4	25	29-35	0.2	0	20	30	25,30
<i>Bull Lake moraine (2285 m asl, 42° 52' 39" N, 109° 51' 00" W)</i>								
Constant	6	140	7.5	1.4	0			
Transient	8	140	6-21	1.2-1.8	0	0.3-10	35,40,50,60	5,10,15, 20,25,30

<sup>a</sup>For a full explanation of range allowed and resolution of each parameter, see Table 3 of Schaller et al. (2009a)

665



**Table 2.**  $^{10}\text{Be}$  Concentrations and GSD<sup>a</sup> in Depth Profiles from Pinedale and Bull Lake Moraines

Sample <sup>b</sup>	Depth (cm)	Sand (wt %)	Silt (wt%)	Clay (wt %)	<i>In situ</i> $^{10}\text{Be}$ concentration <sup>c</sup> ( $10^5$ atoms $\text{g}^{-1}$ )	Meteoric $^{10}\text{Be}$ sample weight (g)	$^9\text{Be}$ carrier weight (mg)	Meteoric $^{10}\text{Be}$ concentration <sup>c</sup> ( $10^6$ atoms $\text{g}^{-1}$ )	Meteoric $^{10}\text{Be}$ inventory <sup>d</sup> ( $10^6$ atoms $\text{cm}^{-2}$ )
<i>Pinedale moraine (2262 m asl, 42° 53' 26" N, 109° 49' 34" W)</i>									
04-WRMP-014	3 ± 2	75	18	6	3.67 ± 0.14	4.5747	0.2146	171.283 ± 5.142	1006 ± 30
04-WRMP-013	10 ± 5	68	22	10	3.73 ± 0.09	3.1697	0.2146	199.526 ± 5.986	2743 ± 84
04-WRMP-012	20 ± 10	70	23	7	3.60 ± 0.15	6.4287	0.2146	33.007 ± 3.183	588 ± 64
04-WRMP-011	30 ± 10	74	22	4	3.60 ± 0.08	6.1094	0.2148	16.819 ± 1.541	265 ± 31
04-WRMP-010	43 ± 10	76	19	5	-	5.1606	0.2144	15.357 ± 1.189	306 ± 31
04-WRMP-009	58 ± 10	82	15	3	2.44 ± 0.07	5.6470	0.2146	3.966 ± 0.336	11 ± 10
04-WRMP-008	73 ± 10	85	12	3	-	5.4438	0.2142	4.673 ± 0.382	33 ± 11
04-WRMP-007	88 ± 10	81	16	3	1.89 ± 0.09	5.6027	0.2140	6.699 ± 0.563	94 ± 17
04-WRMP-006	103 ± 10	82	15	3	-	6.0067	0.2103	3.569 ± 0.322	0 ± 10
04-WRMP-005	118 ± 10	71	23	6	-	3.0500	0.2127	6.207 ± 0.284	79 ± 9
04-WRMP-004	133 ± 10	71	24	5	1.11 ± 0.03	3.1070	0.2134	6.489 ± 0.302	88 ± 9
04-WRMP-003	148 ± 10	74	21	6	-	2.9340	0.2128	5.656 ± 0.249	63 ± 7
04-WRMP-002	163 ± 10	72	22	6	-	2.8869	0.2107	5.531 ± 0.240	59 ± 7
04-WRMP-001	180 ± 10	72	23	6	-	3.0824	0.2135	5.098 ± 0.236	52 ± 8
]									5387 ± 122
<i>Bull Lake moraine (2285 m asl, 42° 52' 39" N, 109° 51' 00" W)</i>									
AT-FL-4L	5 ± 2	69	22	9	14.9 ± 0.9	1.0174	0.4125	415.475 ± 12.464	4092 ± 125
AT-FL-4K	20 ± 5	51	29	20	14.8 ± 0.7	1.0793	0.2139	298.813 ± 8.965	8774 ± 269
AT-FL-4J	28 ± 5	52	34	14	14.0 ± 0.6	1.0824	0.2140	230.442 ± 6.913	3585 ± 111
AT-FL-4I	43 ± 5	47	23	30	12.3 <sup>v</sup> ± 0.7	1.0593	0.1963	26.590 ± 0.798	608 ± 24
AT-FL-4H	53 ± 5	50	28	22	-	1.0176	0.2141	11.433 ± 0.343	102 ± 7
AT-FL-4G	64 ± 5	54	26	20	9.08 ± 0.56	1.0109	0.2144	7.083 ± 0.382	17 ± 8
AT-FL-4F	79 ± 10	60	24	16	8.50 ± 0.48	1.01	0.2141	6.639 ± 0.236	10 ± 7
AT-FL-4E	89 ± 10	62	24	14	-	1.0722	0.2142	6.318 ± 0.246	0 ± 5
AT-FL-4D	94 ± 10	75	17	9	-	-	-	6.723 <sup>e</sup>	4 <sup>e</sup>

AT-FL-4C	104 ± 10	64	26	10	5.98 <sup>□</sup> ± 1.00	1.0164	0.2144	7.129 ± 0.428	16 ± 9
AT-FL-4B	114 ± 10	60	25	15	-	1.0283	0.2142	8.021 ± 0.241	34 ± 5
AT-FL-4A	130 ± 10	60	25	15	4.93 ± 0.28	1.0294	0.2143	8.449 ± 0.253	68 ± 8
∫									17310 ± 318

<sup>a</sup>Grain size distributions and *in situ* <sup>10</sup>Be concentrations from Schaller et al. (2009a)

<sup>b</sup>See Schaller et al. (2009a) for the grain size fraction analyzed for each sample

<sup>c</sup>Corrected for blank, reported error includes analytical uncertainties (1σ)

<sup>d</sup>Corrected for inheritance

<sup>e</sup>Average of <sup>10</sup>Be<sub>met</sub> concentrations from directly above and below this depth

<sup>□</sup>Average of multiple aliquots analyzed in Schaller et al. (2009a)

**Table 3.** <sup>10</sup>Be<sub>met</sub> flux estimates, raw and normalized for Holocene paleointensity variations

Method	F( <sup>10</sup> Be <sub>met</sub> ) uncorrected (x 10 <sup>6</sup> atoms cm <sup>-2</sup> y <sup>-1</sup> )	Valid over time scale (ky)	<sup>10</sup> Be <sub>met</sub> production ratio relative to Modern	<sup>10</sup> Be <sub>met</sub> production ratio relative to Holocene	F( <sup>10</sup> Be <sub>met</sub> ) corrected to represent Holocene (x 10 <sup>6</sup> atoms cm <sup>-2</sup> y <sup>-1</sup> )
Pinedale (This Study)	1.04 (±0.14)	6	0.88 <sup>a</sup>	0.71 <sup>a</sup>	1.46 (±0.20)
Bull Lake (This Study)	1.04 (±0.39)	24	0.99 <sup>a</sup>	0.80 <sup>a</sup>	1.30 (±0.48)
Graly et al. (2011)	0.55 (± 0.05)	0.005	0.82 <sup>b</sup>	0.67 <sup>c</sup>	0.83 (±0.08)
Heikkilä and von Blanckenburg (2015)	-	10	1.23 <sup>c</sup>	-	1.38 (+0.99) <sup>d</sup>

<sup>a</sup> using measured <sup>10</sup>Be<sub>met</sub> seafloor accumulation record of Christl et al. (2010) from 6 ky and 24 ky to present for the Pinedale and Bull Lake moraines, respectively

<sup>b</sup> using the paleomagnetic scaling method of Masarik and Beer (2009)

<sup>c</sup> using the paleomagnetic reconstruction method of Steinhilber et al. (2012)

<sup>d</sup> uncertainty represents the difference between the 'industrial' and the 'pre-industrial' modeled flux of Heikkilä and von Blanckenburg (2015)